Hydrazone Ligation Strategy to Assemble Multifunctional Viral Nanoparticles for Cell Imaging and Tumor Targeting

ARTICLE *in* NANO LETTERS · FEBRUARY 2010

Impact Factor: 13.59 · DOI: 10.1021/nl1002526 · Source: PubMed

7 AUTHORS, INCLUDING:

John D Lewis
University of Alberta
91 PUBLICATIONS **1,649** CITATIONS
SEE PROFILE

Nicole F Steinmetz
Case Western Reserve University
79 PUBLICATIONS **1,595** CITATIONS
SEE PROFILE

Marianne Manchester
University of California, San Diego
95 PUBLICATIONS **4,782** CITATIONS
SEE PROFILE

Heidi Stuhlmann
Weill Cornell Medical College
65 PUBLICATIONS **6,054** CITATIONS
SEE PROFILE

NANO LETTERS

pubs.acs.org/NanoLett

Hydrazone Ligation Strategy to Assemble Multifunctional Viral Nanoparticles for Cell Imaging and Tumor Targeting

Florence M. Brunel,[⊥,†,‡] John D. Lewis,[†,#,⊥] Giuseppe Destito,[†,§,∥] Nicole F. Steinmetz,[†,§] Marianne Manchester,[†,§,▽] Heidi Stuhlmann,[†,¶] and Philip E. Dawson*[,†,‡]

[†]Department of Cell Biology, [‡]Department of Chemistry, [§]Center for Integrative Molecular Biosciences (CIMBio), The Scripps Research Institute, La Jolla, California, 92037, and [∥]Dipartmento di Medicina Sperimentale e Clinica, Università degli Studi Magna Graecia di Catanzaro, Viale Europa, Campus Universitario di Germaneto, 88100, Catanzaro, Italy

ABSTRACT Multivalent nanoparticle platforms are attractive for biomedical applications because of their improved target specificity, sensitivity, and solubility. However, their controlled assembly remains a considerable challenge. An efficient hydrazone ligation chemistry was applied to the assembly of Cowpea mosaic virus (CPMV) nanoparticles with individually tunable levels of a VEGFR-1 ligand and a fluorescent PEGylated peptide. The nanoparticles recognized VEGFR-1 on endothelial cell lines and VEGFR1-expressing tumor xenografts in mice, validating targeted CPMV as a nanoparticle platform in vivo.

KEYWORDS Viral nanoparticle, chemical ligation, cell imaging, tumor targeting, VEGFR-1

Noninvasive visualization of complex cellular systems is of growing importance in many areas of research.[1] Given current technologies, intravital imaging of clinically relevant solid tumors remains a challenge due to the specificity, sensitivity, and bioavailability of available agents in vivo. Molecular nanoscaffolds can be used to address these challenges by enabling the multivalent display of targeting ligands, imaging moieties, and other functional groups. The plant virus Cowpea mosaic virus (CPMV) (Figure 1) is a viral nanoparticle (VNP) that has proven to be a robust macromolecular scaffold for numerous applications.[2,3] CPMV is ~30 nm in diameter with a capsid composed of 60 identical copies of the large (L, 41 kDa) and small (S, 24 kDa) capsid proteins.[4] The protein coat can be chemically modified at amino,[5] carboxyl,[6,7] or thiol groups[2] on its exterior surface, enabling a range of chemical and biological modifiers to be attached to the particles.[8]

The general feasibility of using VNPs for applications such as biomedical imaging and targeted drug-delivery has been demonstrated for VNPs such as Cowpea chlorotic mottle virus (CCMV), Potato virus X, Hibiscus chlorotic ringspot virus (HCRSV), and bacteriophages M13, $Q\beta$, and MS2,[9−15] For example, we recently showed that a CPMV-fluorophore conjugate enables global imaging of the entire vasculature in live embryos.[3] Dye-labeled CPMV particles have also been utilized to image sites of inflammation in the central nervous system.[12] Toward targeted and therapeutic approaches, dual-modified targeted VNPs bearing chemotherapeutics or photosensitizers have been developed with the goal of cytotoxic activity.[11,15,13] Covalent modification of VNPs with tumor ligands such as folic acid allows targeting to cancer cells in vitro.[10] Neverthless, targeted delivery of VNPs to specific molecular receptors in vivo has not yet been demonstrated.

Selective targeting and imaging of cells expressing vascular endothelial growth factor receptors (VEGFRs) has potential applications in angiogenesis research, as well as in understanding, detecting, and treating cancer.[16] Because of its upregulation in tumor vasculature, a number of noninvasive imaging strategies have targeted VEGFR-2 (Flk1 or KDR).[17,18] The homologous VEGFR-1 (Flt1) is expressed in breast cancers,[19] gastric cancers,[20] and schwannomas.[21] Importantly, VEGFR-1 has been identified as a tumor-specific vascular endothelial cell surface protein by subtractive proteomic mapping.[22] A VEGFR-1 specific peptide, F56, was discovered through phage display techniques directed against the soluble receptor.[23] This high-affinity peptide has been shown to suppress tumor growth and metastasis in implanted human breast cancer cells (BICR-H1) in an immune-compromised mouse model.[23] These properties suggest that VEGFR-1 directed ligands may be useful for directing VNPs to tumors and tumor vasculature.

* To whom correspondence should be addressed. Phone: (858) 784-7015. Fax: (858) 784-7319. E-mail: dawson@scripps.edu.

[⊥] These authors contributed equally to this paper.

[#] Present address: Translational Prostate Cancer Research Group, London Regional Cancer Program, London, ON, N6A 4L6 Canada.

[▽] Present address: Skaggs School of Pharmacy and Pharmaceutical Sciences, University of California San Diego, La Jolla, CA 92093.

[¶] Present address: Department of Cell and Developmental Biology, Weill Cornell Medical College, New York, NY 10065.

Received for review: 01/22/2010
Published on Web: 02/17/2010

DOI: 10.1021/nl1002526 | *Nano Lett.* **2010,** *10,* 1093–1097

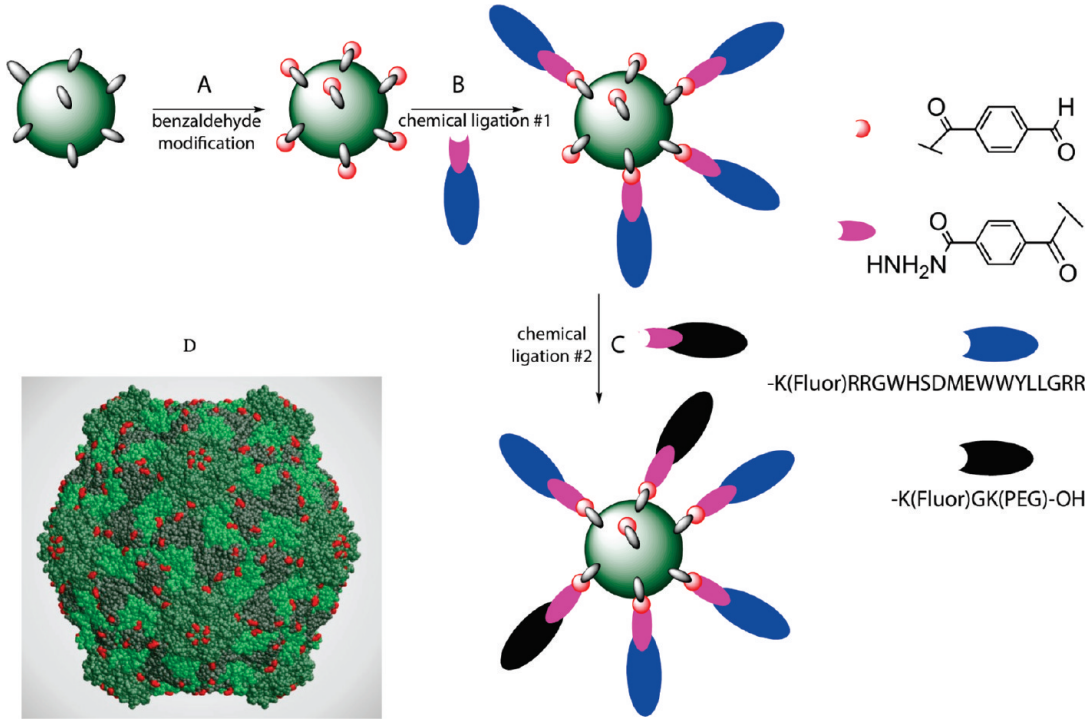

FIGURE 1. CPMV, strategy for labeling the virus capsid. (A) Surface exposed lysines on CPMV are covalently modified with a benzaldehyde group for ligation (red). (B) The hydrazide group (purple) on the ligand F56f (blue) reacts specifically with some of the benzaldehydes on CPMV. (C) A second ligation with hydrazide-PEG500f (black) labels remaining benzaldehyde sites on CPMV, yielding a doubly modified nanoparticle. (D) Three-dimensional structure of CPMV particle showing large subunits (light and dark green) and small subunits (medium green). Lysines available for conjugation are shown in red (image created in RasMol and DeepView using coordinates generated in VIPER[24] from 1NY7.pdb).

TABLE 1. Attachment of Substituents on CPMV[a]

reagents	control C	SFB	PEG P1	PEG P2	PEG P3	PEG P4	F56f F1	F56f PEG FP1	F56f PEG FP2	F56f PEG FP3
fold excess PEG/aldehyde			10	20	50	100		20	50	100
fold excess F56/aldehyde							100	100	100	100
fold excess fluorescein/ aldehyde	2									
substitutions per CPMV	75	280	20	42	125	197	133	149	163	188

[a] The number of substitutions per virus was measured by UV absorption of fluorescein at 495 nm with the exception of SFB, where the absorption was measured at 350 nm. For simplicity, in the table PEG corresponds to PEG500f. For subsequent conjugations, the level of excess substituent added to each reaction is expressed as "fold excess" over the number of attached benzaldehydes.

While it has been possible to conjugate small-molecule ligands to VNPs in a controlled manner, it has been more challenging to control the sequential attachment of more complex macromolecular ligands. To generate CPMV nanoparticles with (1) a fluorescent dye for imaging, (2) a PEG polymer for improved plasma circulation time, and (3) the peptide ligand F56, we developed a stepwise assembly strategy based on an efficient hydrazone ligation chemistry (Figure 1 and Supporting Information, S1; experimental details are given in the Supporting Information). The chemoselective reaction of an arylhydrazide or hydrazine with a benzyaldehyde moiety is rapid in weakly acidic buffer and forms a bisarylhydrazone product that absorbs strongly at ~350 nm. To facilitate the ligation, CPMV was functionalized with a highly reactive, water-soluble 4-formylbenzoyl-sulfoNHS ester to convert exposed lysine residues to benzaldehyde groups (Figure 1). The number of reactive benzaldehyde groups per virion was directly determined by reaction with excess 2-hydrazinopyridine and measuring the absorbance at 350 nm ($\varepsilon = 18\ 000\ M^{-1}\ cm^{-1}$), directly showing that an average of 280 of the 300 available sites on the CPMV particle were modified (Table 1). For subsequent conjugations, the level of excess substituent added to each reaction is expressed as "fold excess" over the number of attached benzaldehyde groups.

Unmodified CPMV particles are rapidly internalized by a wide variety of cell types in vitro and in vivo.[25−27] This uptake is governed primarily by binding to a cell-surface form of the intermediate filament vimentin[25,28] and can be inhibited by PEGylation,[3,10,29] a modification that also increases plasma circulation time and should enhance the accumulation of the nanoparticles in target tissues.[30] For this

DOI: 10.1021/nl1002526 | *Nano Lett.* **2010,** *10,* 1093–1097

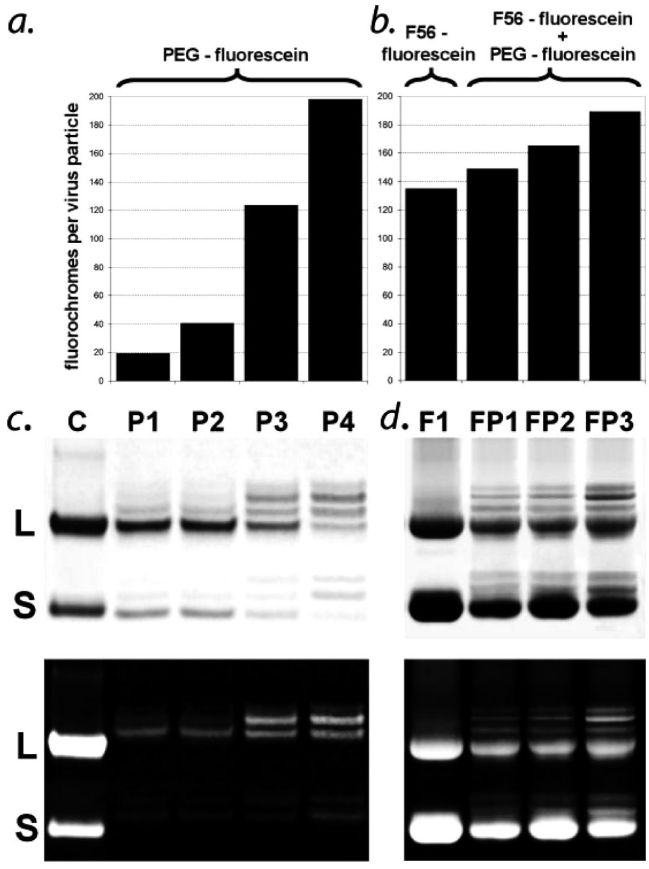

FIGURE 2. CPMV conjugation with F56 peptide-fluorescein and PEG-fluorescein. (a) Relative fluorescence of PEG-conjugated CPMVs; P1, 10-fold excess; P2, 20-fold excess; P3, 50-fold excess; P4, 100-fold excess of PEG500f over benzaldehyde groups. (b) Relative fluorescence of F56f and F56f/PEG500f mixed conjugated CPMVs; F1, 100-fold excess F56f; FP1, 100-fold excess F56f/20-fold excess PEG500f; FP2, 100-fold excess F56f/50-fold excess PEG500f; FP3, 100-fold excess F56f/100-fold excess PEG500f over benzaldehyde groups. (c) SDS-PAGE of CPMV conjugates stained with Coomassie showing large (L) and small (S) subunits. (d) SDS-PAGE of CPMV conjugates by UV transillumination. Lane labels in (b) correspond to those in (a) and (c).

purpose, PEG500f, a nontargeted peptide with a fluorescein, a monodisperse PEG polymer, and a terminal hydrazido group, was synthesized (Supporting Information, Figure S2). PEG500f alone was incubated with benzaldehyde-modified CPMV yielding 20 (**P1**), 42 (**P2**), 125 (**P3**), and 197 (**P4**) molecules of PEG500f per VNP particle, respectively (Figure 2a, Table 1). Further analysis of CPMV-PEG500f conjugates by SDS-PAGE indicated a progressive loading of PEG500f onto the lysines of the large subunit (3) and the small subunit (2) (Figure 2b,c). Using 100 fold-excess of PEG500f per benzaldehyde, an average of two lysines on L and one on S are linked to the fluorophore, in agreement with ~200 fluorophores per viral particle (Figure 2b).

The VEGFR-1-specific F56 peptide is extremely insoluble and had previously been studied only as a fusion protein with dihydrofolate reductase (DHFR).[23] Four arginines (to improve solubility), a fluorescein, and an N-terminal hydrazide were appended to form hydrazido-K(fluorescein)-RRGWHSDMEWWYLLGRR (F56f). This peptide was ligated to benzaldehyde-functionalized CPMV at pH 5.5 through a stable hydrazone linkage. A maximal loading of 133 peptides per particle (**F1**), as measured by fluorescein absorbance, was obtained (Figure 2a and Table 1). The CPMV nanoparticles remained intact in the labeling procedure as monitored by gradient density ultracentrifugation and size exclusion chromatography. The high levels of labeling with the poorly soluble F56f peptide under ambient conditions demonstrates the utility of this hydrazone ligation approach for the functionalization of macromolecules and is comparable to the highest reported loadings of complex targeting molecules onto CPMV.[31]

Since only half of the benzaldehyde moieties on CPMV were modified by the F56f peptide ligand, we reasoned that sequential conjugation of F56f, followed by the more reactive PEG500f, would be possible (Figure 1). Aliquots of the reaction mixture containing F56f-loaded CPMV (130/particle) were supplemented with a 20-, 50-, or 100-fold excess of PEG500f (over benzaldehyde groups) to generate doubly labeled **FP** particles. This procedure resulted in further loading of the CPMV-F56f conjugate with 16 (**FP1**), 30 (**FP2**), or 55 (**FP3**) PEG500f molecules as determined by fluorescein absorbance (Figure 2a, Table 1). Analysis of these conjugates by SDS-PAGE indicated a progressive increase in loading of the CPMV surface with F56f peptide and PEG500f. Using this two-step approach, two peptides were loaded to achieve a total substitution level of over 180/virion. Despite the small Stokes shift of fluorescein, the densely labeled VNPs were highly fluorescent.[32] Importantly, the modular nature of the synthetic procedures described here are compatible with other imaging moieties such as near-infrared fluorescent dyes.

To test the specificity of targeting, Ea.hy926 human endothelial cells that express high levels of VEGFR-1[33] and fibroblasts lacking VEGFR-1 expression[34] were treated with CPMV derivatives (experimental details are given in the Supporting Information). Consistent with previous findings,[35] cell attachment assays using fluorescent microscopy show that low levels of PEG500f (**P1** and **P2**) did not affect the binding affinity of the particles to endothelial cells (Figure 3a). In contrast, particles with high loading, **P3** and **P4**, showed a 55 and 84% reduction in nonspecific binding. The absence of signal in fluorescence imaging experiments with **P4** confirmed minimal binding or internalization into endothelial cells (Figures 3b, 4b).

As shown in Figure 3a, F56f-ligand conjugated CPMV **F1**, bound to human endothelial cells 67% more efficiently than unlabeled virus. This binding was significantly reduced in the presence of free F56f peptide (Supporting Information, Figure S3). Fluorescence microscopy revealed that non-PEGylated **F1** associated significantly with both endothelial cells and fibroblasts (Figure 3b, bottom right). These results confirm that sufficient PEG500f loading is required to achieve specific targeting of VEGFR-1.

DOI: 10.1021/nl1002526 | *Nano Lett.* **2010,** *10,* 1093–1097

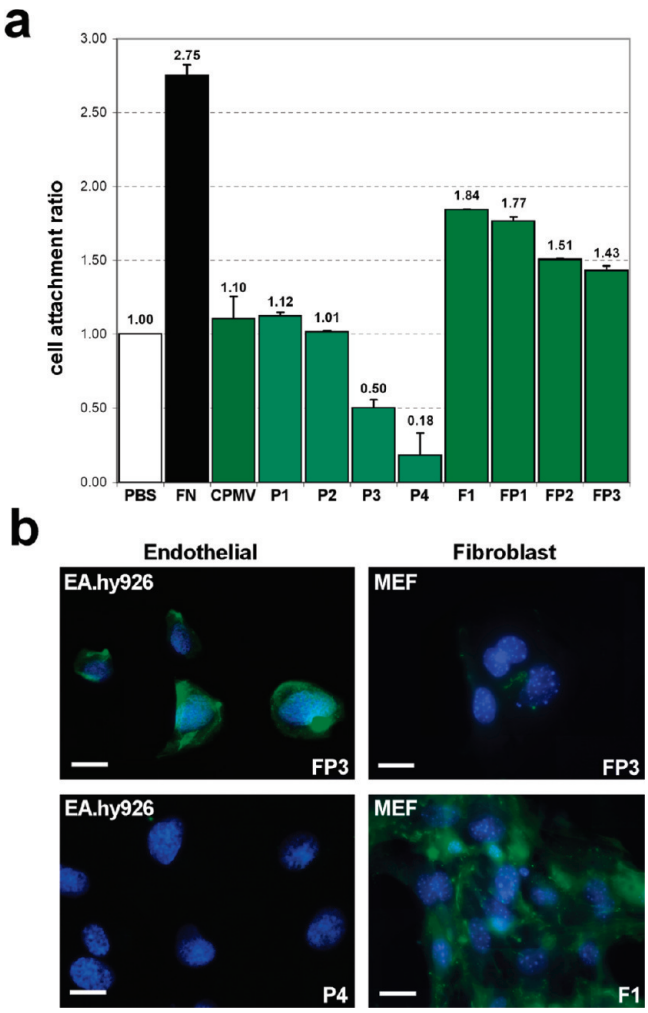

FIGURE 3. Binding of CPMV conjugates to endothelial cells in vitro. (a) Cell adhesion assay with human endothelial cells (AE.hy926). Results are normalized to PBS control (y-axis, binding efficiency: relative binding, normalized to PBS). Assay was performed in duplicate. Positive control, fibronectin (FN); negative control, native CPMV (CPMV); see Table 1 for an explanation of CPMV conjugates. (b) Fluorescence visualization of CPMV conjugates FP3 (loaded with PEG500f and F56f), P4 (loaded with PEG500f only), and F1 (loaded with F55f only) bound to endothelial cells (EA.hy926) and fibroblasts (MEF). CPMV particles are shown in green. Nuclei were stained with DAPI (in blue).

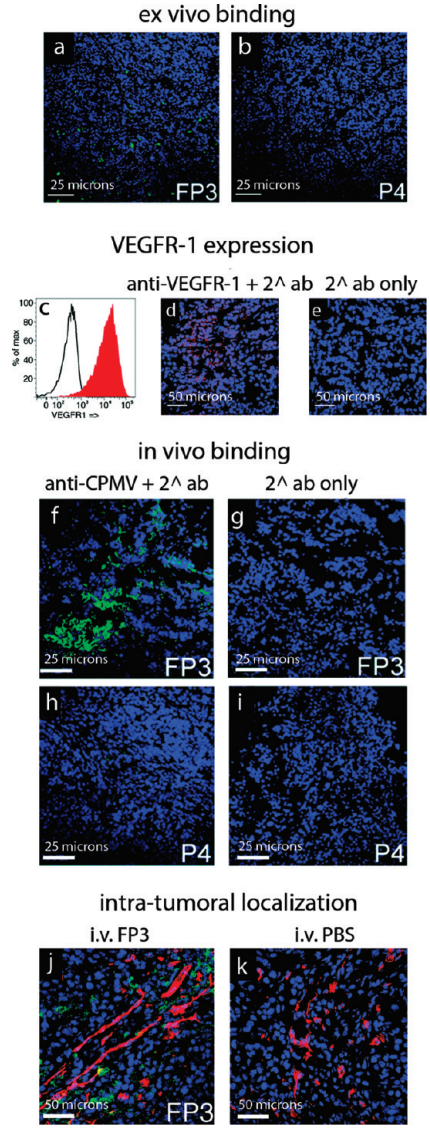

FIGURE 4. Targeting CPMV to tumors in vivo. (a,b) Confocal images showing that FP3 (a), but not P4 nanoparticles (b), bind to tumor tissue. CPMV was stained with fluorescently labeled secondary antibodies. (c) Expression of VEGFR-1 on HT-29 cells in vitro studied by flow cytometry. Red histogram = anti-VEGFR-1 and secondary antibody. Black histogram = secondary antibody only. (d,e) HT-29 tumors stained ex vivo with anti-VEGFR-1 antibodies (d) or secondary antibody only (e). (f−i) FP3 or P4 particles localize within HT-29 tumor xenografts following intravenous administration in nude/WEHI mice. CPMV was stained using specific antibodies. (j,k) Intratumoral localization of particles (green) and endothelial cells (red) following intravenous administration of FP3 (j) or PBS (k). CPMV was stained using specific antibodies, and endothelial cells were stained using anti-CD31 antibody. Blue = DAPI stain to indicate cell nuclei.

To further evaluate the specificity of PEGylated, VEGFR-1 targeted particles, the dual-labeled nanoparticle **FP3** was visualized by confocal fluorescence microscopy. We found that the **FP3** nanoparticles did not bind to fibroblasts (Figure 3b top right) but bound VEGFR-1 expressing EA.hy926 endothelial cells in a specific manner (Figure 3b top left, Figure 4a). These results strongly suggest that VEGFR-1 peptide F56f can effectively target CPMV nanoparticles to endothelial cells, and that the addition of PEG significantly reduces nonspecific binding.

We next evaluated the tumor specificity of targeted **FP3** and untargeted **P4** nanoparticles by examining their ability to bind selectively to HT-29 (human colon carcinoma) tumor sections ex vivo. Using confocal microscopy imaging, significant binding to the tumor sections was observed with **FP3** but not with **P4** (Figure 4a,b). Nanoparticles containing F56f-ligand but lacking PEG500f (**F1**) also bound the HT-29 tumor cells, but nonspecific binding was also observed, as expected (data not shown).

To determine whether VEGFR-1-targeted CPMV nanoparticles could localize to tumors in vivo, nude/WEHI mice

DOI: 10.1021/nl1002526 | *Nano Lett.* **2010,** *10,* 1093–1097

bearing HT-29 tumors, which express high levels of VEGFR-1 (Figure 4c–e), were inoculated intravenously with either **FP3** or **P4**, and the particles were allowed to circulate for two hours before the tumors were excised. CPMV was detected by immunofluorescence staining and confocal microscopy (see Supporting Information for experimental details). No uptake was detected in tumors isolated from mice administered with **P4** (Figure 4h,i). In contrast, **FP3** accumulated throughout the tumor tissue (Figure 4j,k). These results suggest that multifunctional nanoparticles can target tumors in vivo but do not necessarily accumulate on the endothelial cells lining the tumor vessels (Figure 4j). The somewhat unexpected extravasation of the targeted nanoparticles may be explained by the inherent leakiness of the tumor vasculature known as the enhanced permeability and retention effect (EPR),[36] as well as the expression of VEGFR-1 on both the endothelial and tumor cells.

In summary, we have developed a hydrazone ligation chemical strategy to generate a multivalent CPMV nanoparticle that specifically targets VEGFR-1. We developed targeted VNPs comprised of 133 copies of VEGFR-1 ligand, 55 copies of a PEGylated peptide, and a total of 188 fluorescent dyes. Importantly, the hydrazone ligation strategy enables the sequential introduction of different peptides in a ratio that is controlled by the reaction conditions, and the modular nature of the chemistry can be tailored for specific applications. For example, to use these nanoparticles for in vivo imaging it will be necessary to use an alternate imaging moiety with improved tissue penetration characteristics. The hydrazone ligation strategy enables design of these uniquely multifunctional CPMV nanoparticles, which may be further developed into powerful tools for the detection and the monitoring of treatment of cancer and other diseases.

Acknowledgment. This study was supported by NIH Grants P01 HD09402 and R01 GM059380 to P.E.D.; R01 HL 068648 to H.S.; R01 CA112075 to M.M., K99 EB009105 to N.F.S.; as well as CIHR MOP-84535 to J.D.L., American Heart Association Postdoctoral Fellowship (to N.F.S.), and AmfAR fellowship to F.B.

Supporting Information Available. Experimental details and figures are given. This material is available free of charge via the Internet at http://pubs.acs.org.

REFERENCES AND NOTES

(1) Ntziachristos, V.; Ripoll, J.; Wang, L. V.; Weissleder, R. *Nat. Biotechnol.* **2005**, *23* (3), 313–20.
(2) Wang, Q.; Lin, T.; Johnson, J. E.; Finn, M. G. *Chem. Biol.* **2002**, *9* (7), 813–9.
(3) Lewis, J. D.; Destito, G.; Zijlstra, A.; Gonzalez, M. J.; Quigley, J. P.; Manchester, M.; Stuhlmann, H. *Nat. Med.* **2006**, *12* (3), 354–360.
(4) Lin, T.; Chen, Z.; Usha, R.; Stauffacher, C. V.; Dai, J. B.; Schmidt, T.; Johnson, J. E. *Virology* **1999**, *265* (1), 20–34.
(5) Chatterji, A.; Ochoa, W.; Paine, M.; Ratna, B. R.; Johnson, J. E.; Lin, T. *Chem. Biol.* **2004**, *11* (6), 855–63.
(6) Chatterji, A.; Ochoa, W. F.; Paine, M.; Ratna, B. R.; Johnson, J. E.; Lin, T. W. *Chem. Biol.* **2004**, *11* (6), 855–863.
(7) Steinmetz, N. F.; Lomonossoff, G. P.; Evans, D. J. *Langmuir* **2006**, *22* (8), 3488–90.
(8) Steinmetz, N. F.; Evans, D. J. *Org. Biomol. Chem.* **2007**, *5* (18), 2891–902.
(9) Brown, W. L.; Mastico, R. A.; Wu, M.; Heal, K. G.; Adams, C. J.; Murray, J. B.; Simpson, J. C.; Lord, J. M.; Taylor-Robinson, A. W.; Stockley, P. G. *Intervirology* **2002**, *45* (4–6), 371–80.
(10) Destito, G.; Yeh, R.; Rae, C. S.; Finn, M. G.; Manchester, M. *Chem. Biol.* **2007**, *14* (10), 1152–62.
(11) Ren, Y.; Wong, S. M.; Lim, L. Y. *Bioconjug. Chem.* **2007**, *18* (3), 836–43.
(12) Shriver, L. P.; Koudelka, K. J.; Manchester, M. *J. Neuroimmunol.* **2009**.
(13) Steinmetz, N. F.; Hong, V.; Spoerke, E. D.; Lu, P.; Breitenkamp, K.; Finn, M. G.; Manchester, M. *J. Am. Chem. Soc.* **2009**, *131* (47), 17093–5.
(14) Steinmetz, N. F.; Mertens, M. E.; Taurog, R. E.; Johnson, J. E.; Commandeur, U.; Fischer, R.; Manchester, M. *Nano Lett*, in press.
(15) Suci, P. A.; Varpness, Z.; Gillitzer, E.; Douglas, T.; Young, M. *Langmuir* **2007**, *23* (24), 12280–6.
(16) Kargiotis, O.; Rao, J. S.; Kyritsis, A. P. *J. Neurooncol.* **2006**, *78* (3), 281–93.
(17) Backer, M. V.; Levashova, Z.; Patel, V.; Jehning, B. T.; Claffey, K.; Blankenberg, F. G.; Backer, J. M. *Nat. Med.* **2007**, *13* (4), 504–9.
(18) Cai, W.; Chen, K.; Mohamedali, K. A.; Cao, Q.; Gambhir, S. S.; Rosenblum, M. G.; Chen, X. *J. Nucl. Med.* **2006**, *47* (12), 2048–56.
(19) Lee, T. H.; Seng, S.; Sekine, M.; Hinton, C.; Fu, Y.; Avraham, H. K.; Avraham, S. *PLoS Med.* **2007**, *4* (6), No. e186.
(20) Yamaguchi, T.; Bando, H.; Mori, T.; Takahashi, K.; Matsumoto, H.; Yasutome, M.; Weich, H.; Toi, M. *Cancer Sci.* **2007**, *98* (3), 405–10.
(21) Uesaka, T.; Shono, T.; Suzuki, S. O.; Nakamizo, A.; Niiro, H.; Mizoguchi, M.; Iwaki, T.; Sasaki, T. *J. Neurooncol.* **2007**, *83* (3), 259–66.
(22) Oh, P.; Li, Y.; Yu, J.; Durr, E.; Krasinska, K. M.; Carver, L. A.; Testa, J. E.; Schnitzer, J. E. *Nature* **2004**, *429* (6992), 629–35.
(23) An, P.; Lei, H.; Zhang, J.; Song, S.; He, L.; Jin, G.; Liu, X.; Wu, J.; Meng, L.; Liu, M.; Shou, C. *Int. J. Cancer* **2004**, *111* (2), 165–73.
(24) Reddy, V. S.; Natarajan, P.; Okerberg, B.; Li, K.; Damodaran, K. V.; Morton, R. T.; Brooks, C. L., III; Johnson, J. E. *J. Virol.* **2001**, *75* (24), 11943–7.
(25) Koudelka, K. J.; Destito, G.; Plummer, E. M.; Trauger, S. A.; Siuzdak, G.; Manchester, M. *PLoS Pathog.* **2009**, *5* (5), No. e1000417.
(26) Lewis, J. D.; Destito, G.; Zijlstra, A.; Gonzalez, M. J.; Quigley, J. P.; Manchester, M.; Stuhlmann, H. *Nat. Med.* **2006**, *12* (3), 354–60.
(27) Gonzalez, M. J.; Plummer, E. M.; Rae, C. S.; Manchester, M. *PLoS One* **2009**, *4* (11), No. e7981.
(28) Koudelka, K. J.; Rae, C. S.; Gonzalez, M. J.; Manchester, M. *J. Virol.* **2007**, *81* (4), 1632–40.
(29) Steinmetz, N. F.; Manchester, M. *Biomacromolecules* **2009**, *10* (4), 784–92.
(30) Okuda, T.; Kawakami, S.; Akimoto, N.; Niidome, T.; Yamashita, F.; Hashida, M. *J. Controlled Release* **2006**, *116* (3), 330–6.
(31) Sen Gupta, S.; Kuzelka, J.; Singh, P.; Lewis, W. G.; Manchester, M.; Finn, M. G. *Bioconjug. Chem.* **2005**, *16* (6), 1572–9.
(32) Soto, C. M.; Blum, A. S.; Vora, G. J.; Lebedev, N.; Meador, C. E.; Won, A. P.; Chatterji, A.; Johnson, J. E.; Ratna, B. R. *J. Am. Chem. Soc.* **2006**, *128* (15), 5184–9.
(33) Fu, J. X.; Wang, W.; Bai, X.; Wang, L.; Zhu, Z. L.; Chen, Z. X.; Ruan, C. G. *Aizheng* **2002**, *21* (11), 1217–21.
(34) Morishita, K.; Johnson, D. E.; Williams, L. T. *J. Biol. Chem.* **1995**, *270* (46), 27948–53.
(35) Steinmetz, N. F.; Manchester, M. *Biomacromolecules* **2009**, *10* (4), 784–92.
(36) Iyer, A. K.; Khaled, G.; Fang, J.; Maeda, H. *Drug Discovery Today* **2006**, *11* (17–18), 812–8.

DOI: 10.1021/nl1002526 | *Nano Lett.* **2010,** *10,* 1093–1097